Available online at www.sciencedirect.com
ScienceDirect
Trans. Nonferrous Met. Soc. China 35(2025) 3161−3178
Transactions of Nonferrous Metals Society of China
www.tnmsc.cn

Pilot-scale case study on vanadium extraction from vanadium-bearing shale using suspension oxidation roasting−curing−leaching process

Zhe BAI[1,2,3], Jia-hao HE[1,2], Ming-xing WANG[1,2],
Yue-xin HAN[1,2], Yong-sheng SUN[1,2], Shuai YUAN[1,2], Jian-ping JIN[1,2]

1. State Key Laboratory of Mineral Processing, Northeastern University, Shenyang 110819, China;
2. School of Resources and Civil Engineering, Northeastern University, Shenyang 110819, China;
3. Engineering Research Center of Frontier Technologies for Low-carbon Steelmaking (Ministry of Education), Shenyang 110819, China

Received 23 September 2024; accepted 12 June 2025

Abstract: Addressing the environmental issues of traditional vanadium extraction methods from vanadium-bearing shale, a highly efficient and clean suspension oxidation roasting−curing−leaching process was proposed and semi-industrial trials were conducted. Vanadium in raw ore mainly exists in sericite, roscoelite, and limonite, predominantly in the forms of V(III) and V(IV). Under the conditions of a feed rate of 30 kg/h, an air flow rate of 28.0 m^3/h, an O_2 flow rate of 4.0 m^3/h, and a temperature of 900 °C in both the suspension furnace and fluidized reactor, the vanadium-bearing mica underwent dehydroxylation and transformed into illite−montmorillonite. These changes disrupted the crystal structure of mica, facilitating vanadium extraction. Compared to direct acid leaching, curing-leaching demonstrates better performance in vanadium extraction. Under the conditions of curing temperature of 130 °C, acid dosage of 40 wt.%, curing time of 6 h, and leaching time of 3 h, a V_2O_5 leaching efficiency of 83.92% was achieved.

Key words: V-bearing shale; suspension roasting; curing-leaching; pilot case; mineralogy

1 Introduction

Vanadium (V) is one of the rare strategic metals with multiple valence states [1,2]. Due to its high melting point, ductility, hardness, and corrosion resistance, it is widely utilized in aerospace, chemical industry, batteries, steel alloys, and other fields [3,4]. The rapid development of global strategic emerging industries has led to a substantial increase in demand for vanadium products. This trend has prompted increased focus on the development and utilization of vanadium resources [5−7]. Major countries including China, the United States, Japan, and the European Union, have classified vanadium as a strategic metal essential for national security [8,9].

China possesses the largest vanadium ore reserves globally and also ranks as the world's top exporter of vanadium products [10,11]. Vanadium extraction primarily relies on vanadium slag and V-bearing shale as raw materials [1]. 87% of vanadium resources are contained in V-bearing shale, which is 6.7 times the amount found in vanadium titanium−magnetite [12]. However, fewer than 40% of the exported vanadium products utilize V-bearing shale as a raw material [13]. V-bearing shale, a strategic resource unique to China for the production of vanadium products, offers substantial economic benefits and social value through the

Corresponding author: Jia-hao HE, Tel: +86-13840557731, E-mail: jiahao_he_neu@163.com
https://doi.org/10.1016/S1003-6326(25)66873-7

recovery of valuable metallic vanadium. Vanadium-bearing shale, also known as stone coal, has vanadium content ranging from 0.13% to 2%, classifying it as a low-grade vanadium mineral [14,15]. The mineral composition of V-bearing shale is complex, and depending on the degree of oxidation or weathering, it can be classified into primary and oxidized types [16]. China possesses substantial reserves of primary V-bearing shale; however, the extraction process is challenging because the vanadium predominantly exists as isomorphic V(III) within mica minerals.

Currently, common methods for vanadium extraction from V-bearing shale include direct acid leaching with fluorine-containing leaching aids and salt-enhanced roasting followed by leaching. To address the high acid consumption and low leaching efficiency in direct acid leaching, researchers [17,18] have proposed the addition of leaching aids. ZHENG et al [19−21] developed a complete hydrometallurgical process for extracting vanadium and demonstrated the enhancing effects of fluorine-containing leaching aids on vanadium extraction. CHEN et al [22−24] used ultrasound combined with CaF_2 to enhance the vanadium extraction, further increasing the leaching efficiency. However, the addition of fluorine-containing leaching aids results in the release of hydrogen fluoride (HF), posing significant challenges in industrial production, such as equipment damage and unsafe working environments. Sodium salts, calcium salts, and their composites are common additives in roasting [25,26]. HU and ZHANG [27] achieved a vanadium leaching efficiency of 80%−85% using a Na_2CO_3/NaCl composite salt in roasting. WANG et al [28] employed a CaF_2/CaO composite salt roasting−acid leaching process to extract vanadium from V-bearing shale, achieving a leaching efficiency of 86.74%. Composite salt roasting can effectively disrupt the crystal structure of V-bearing minerals, enhancing vanadium leaching. Although it is an efficient method for extracting vanadium, it has drawbacks such as poor adaptability and significant environmental pollution. Other treatment methods include pressurized acid leaching [29,30] and bioleaching [31−33], with the former using precisely controlled equipment to achieve a vanadium recovery rate of 77%. The latter has a long processing cycle and is still in the early stage of research [26].

Compared to the aforementioned processes, blank roasting (oxidizing roasting) followed by leaching is gaining increasing attention as a green and sustainable vanadium extraction technique. Compared to salt roasting, oxidizing roasting enhances vanadium leaching efficiency by raising the temperature to a certain level, without requiring additional acid consumption. Building on this, many researchers have investigated fluidized roasting to improve vanadium extraction from V-bearing shale [10,34−37]. Fluidized roasting improves the heat exchange between gases and suspended particles, significantly enhancing the heat and mass transfer of powder particles, thereby achieving superior performance metrics [38]. BAI et al [12,39,40] proposed a two-stage fluidized roasting process for V-containing shale with a high carbon content, resulting in a 13.54% increase in vanadium leaching efficiency compared to the original NaCl roasting. In summary, while the oxidizing roasting−leaching process has proven to be a clean and efficient technique for vanadium extraction at the laboratory scale, studies at the semi-industrial scale are still lacking.

The sulfuric acid curing leaching process offers advantages such as low energy consumption, low pollution, and high efficiency, making it a current focus of research in hydrometallurgy [41]. Significant progress has been made, particularly in the application of low-temperature sulfuric acid curing leaching for vanadium extraction from vanadium-bearing shale [42]. Using this method, most refractory vanadium-bearing shale can be effectively treated through water leaching following heat preservation curing. The curing process operates at a low reaction temperature, with minimal carbon decomposition and a short reaction time [43]. This significantly enhances production efficiency. Therefore, further investigation of the curing process is warranted. To date, there have attempts to treat vanadium-bearing shale using suspended oxidation roasting or curing leaching processes independently. However, research combining suspended oxidation roasting and curing leaching for vanadium extraction from vanadium-bearing shale remains scarce. Furthermore, most current studies are primarily laboratory-scale, with limited exploration of pilot-scale processes.

Therefore, this study focused on vanadium-bearing shale from Pingtaishan in Gansu Province,

conducting pilot-scale suspended oxidation roasting trials. A comparative analysis was conducted between the direct leaching process and curing-leaching process for the roasted products. Detailed process mineralogical analyses were conducted on the vanadium-bearing shale, its roasted products, and the residues from curing leaching, including chemical elements, valence states and occurrence mode of vanadium, mineral composition, and the embedded features of V-bearing minerals. Based on the mineralogical characterization results, the mechanisms underlying vanadium extraction enhancement via suspension-oxidizing roasting pretreatment are systematically investigated, along with evaluating its semi-industrial feasibility. This research aims to bridge process mineralogy with vanadium extraction techniques, thereby providing a theoretical foundation for industrial-scale implementation.

2 Experimental

2.1 Sampling and research methodology

The experimental samples were sourced from the Pingtaishan mining area in Dunhuang, and their characteristics are detailed in Section 3.1. The experiments were conducted using an innovative suspension oxidation roasting (SOR) pilot platform, as shown in Figs. 1(a, b). The equipment used for acid curing and leaching is illustrated in Fig. 1(c). The entire SOR system was computer-controlled, with precise regulation of internal temperature and pressure achieved via thermocouples and pressure sensors. Materials were transferred from the storage bin to the cyclone separator, with the feed speed controlled by a loss-in-mass scale. The materials were then introduced into the suspension furnace for pre-oxidation at 900 °C and underwent secondary oxidation within the fluidized bed reactor at the same temperature to obtain the roasted product. Air was introduced at the bottom of the reactor to oxidize the carbon and volatile components in V-bearing shale, convert lower-valence vanadium to a higher valence, and disrupt the crystal lattice of vanadium-bearing minerals such as mica and tourmaline, thereby enhancing subsequent vanadium leaching. Finally, after passing through the cooler, the products were collected in the product bin.

After initial dedusting in a cyclone separator, the exhaust gases entered heat exchanger I, where they were cooled to 160 °C before being purified in a dust collector. The gases were then cooled to below 50 °C in heat exchanger II and vented to the atmosphere via the Roots blower. The dust from the high-temperature dust collector and the baghouse filter was collected in dust bins, cleaned every 2 h, and manually returned to the storage bin. The entire

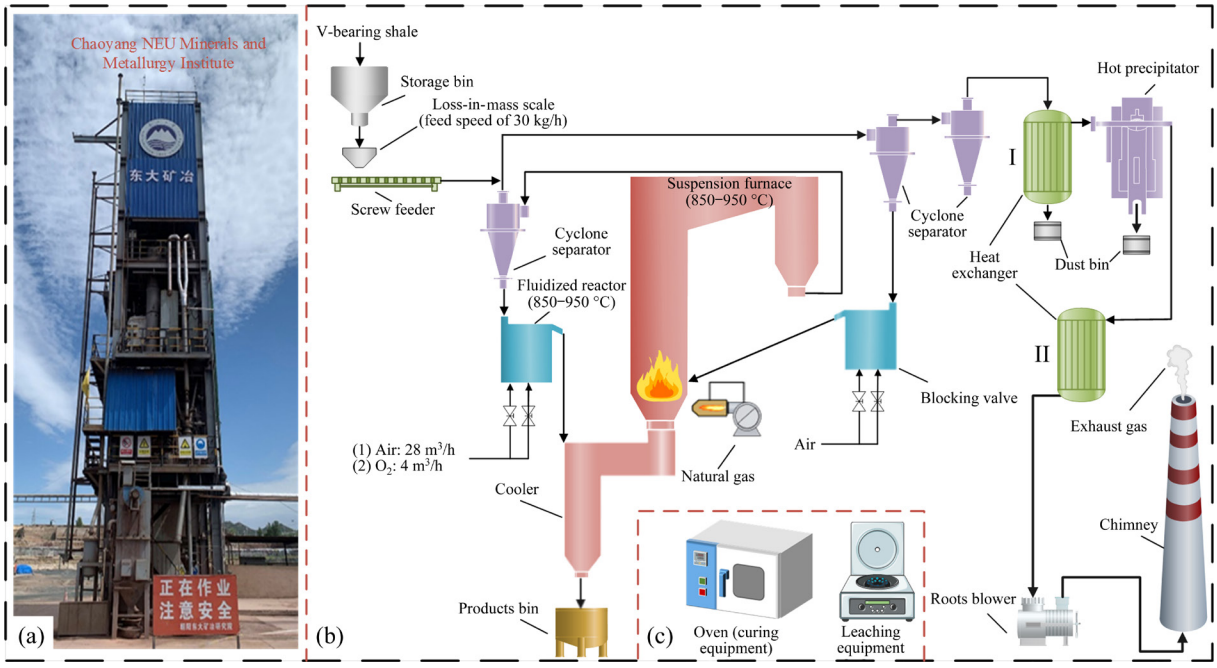

Fig. 1 (a) Photo of pilot-scale roasting equipment; (b) Schematic diagram of pilot-scale SOR system; (c) Schematic diagram of leaching system

SOR system operated under negative pressure, powered by a Roots blower to facilitate the movement of particles and gases. The roasting process was intelligent, energy-efficient, safe, and environmentally sustainable.

The direct leaching (DL) process is described as follows. Initially, 125 mL of deionized water was added to a beaker, followed by a specific amount (30−50 wt.%) of sulfuric acid. After thorough mixing, 100 g of the roasted products were introduced. The beaker was then placed in a 90 °C constant-temperature water bath and stirred for a designated time (3−10 h). Subsequently, the slurry was filtered and dried, and both the mass of the leach residue and the V_2O_5 content were determined.

The acid curing−leaching (CL) process is as follows. 100 g of the roasted products were placed in a wide-mouth bottle to which 15 mL of deionized water and a specific amount (30−50 wt.%) of sulfuric acid were added. After thorough stirring, the mixture was placed in an oven to maintain a specified temperature (100−160 °C). After reaching the predetermined time (4−8 h), 1.1 mL of sulfuric acid and 150 mL of water were added to the bottle. The mixture was then stirred for a specific time (2−5 h) under a stirrer. Subsequently, the mixture was filtered and dried, and both the mass of the leach residue and the V_2O_5 content were determined. In the aforementioned processes, the concentrated sulfuric acid used was of analytical grade, with a content of 98.3 wt.%.

The leaching efficiency (L) of V_2O_5 in V-bearing shale was calculated as follows:

$$L=\left(1-\frac{m_1\alpha_1}{m_2\alpha_2}\right)\times 100\% \quad (1)$$

where m_1 and m_2 are the masses of the leach residue and the roasted products, respectively; α_1 and α_2 are the V_2O_5 grades of the leach residue and the roasted products, respectively.

2.2 Analytical methods

The analytical methods used for determining each chemical composition in this study are detailed in Table 1. The mineral content of the raw ore was determined using a mineral liberation analyzer (MLA, FEI MLA 650). The micromorphologies of the samples were examined using scanning electron microscopy (SEM, Apreo 2C). Phase transformations of the products were analyzed using X-ray diffraction (XRD, X'Pert3 Powder) with a test angle range from 5° to 95° and a scanning speed of 5 (°)/min. The pore structures of the products were characterized through surface area measurements (Quantachrome Nova 2000e). Changes in functional groups within the product were analyzed using a Fourier transform infrared (FT-IR) spectrometer (Nicolet iS50).

Table 1 Methods for determining chemical composition of samples [36,44,45]

Chemical composition	Analytical method
Total iron (TFe)	Titanium(III) chloride reduction potassium dichromate titration methods (routine methods)
V_2O_5	Ferrous amine sulfate titration
SiO_2	Silicomolybdic blue spectrophotometric method reduced by ammonium ferrous sulfate
P	Bismuth phosphomolybdate blue spectrophotometric method
C, S	High frequency combustion with infrared absorption method (CS230-Series carbon/sulfur determinator, LECO, America)
Al_2O_3	EDTA titration
CaO, MgO, TiO_2, K, Na	Flame atomic absorption spectrometric method (iCE™ 3500 AAS Atomic Absorption Spectrometer, Thermo Scientific™, America)

3 Results and discussion

3.1 Process mineralogical characteristics of V-bearing stone coal

3.1.1 Chemical and mineral composition

Table 2 and Fig. 2 illustrate the chemical and mineral compositions of the V-bearing shale. As shown in Table 2, the primary valuable component, V_2O_5, is present at 0.93 wt.%. The impurity components, SiO_2 and Al_2O_3, are present at 58.79 and 7.17 wt.%, respectively. The total carbon content is 12.40 wt.%, with a loss on ignition (LOI) of 18.23 wt.%. The harmful element sulfur is notably high at 0.44 wt.%. Figure 2(a) shows that the principal V-bearing minerals in raw ore are sericite, roscoelite, and limonite, with respective contents of 22.64, 8.35, and 3.17 wt.%. Quartz is the primary gangue mineral and also the most

Table 2 Chemical composition of V-bearing shale (wt.%)

Al_2O_3	SiO_2	V_2O_5	TiO_2	C	TFe	MgO	CaO	P	S	K	Na	LOI
7.17	58.79	0.93	0.74	12.40	2.82	1.19	3.31	0.28	0.44	1.64	0.56	18.23

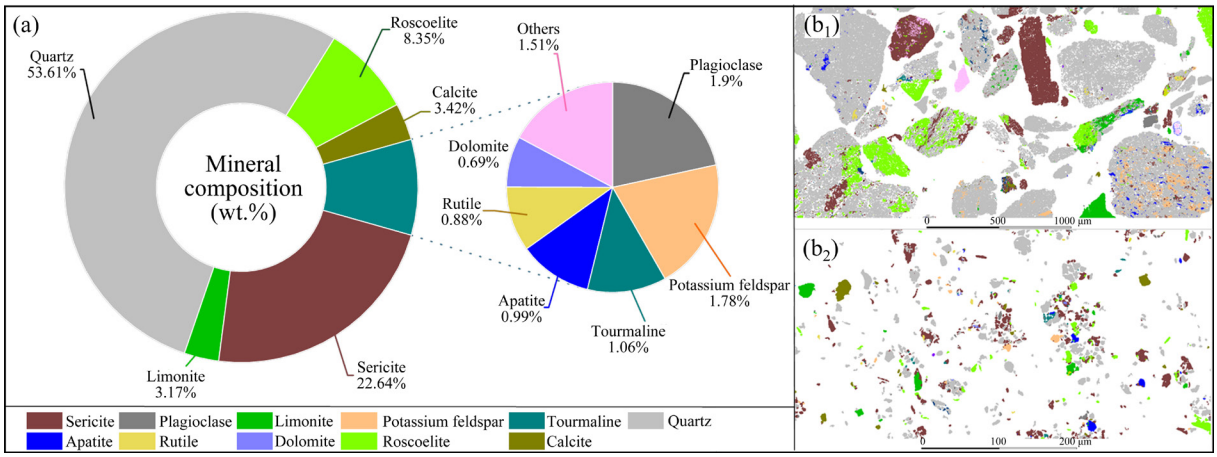

Fig. 2 (a) Mineral composition; (b1) Mineral phase diagram, >38 μm; (b2) Mineral phase diagram , <38 μm

abundant, comprising 53.61 wt.% of the ore. Figure 2(b) illustrates the complex intergrowth relationships among the different minerals.

3.1.2 Vanadium occurrence state

The occurrence state of valuable elements in the ore influences both the difficulty of extraction and the choice of method. The predominant occurrence states of vanadium are adsorption and isomorphism. Vanadium adsorbed on the surfaces of iron oxides and clay minerals can be directly leached with acid [46]. However, vanadium is often present in the form of V(III), substituting for Al(III) in mica, making it difficult to extract without roasting or HF pretreatment [41,47]. Moreover, only V(IV) and V(V) are soluble in the acidic solutions [20]. Therefore, the key to enhancing vanadium extraction lies in disrupting the crystal lattice structure and oxidizing the lower-valence vanadium [48]. Figure 3 illustrates the phase and valence state of vanadium in raw ore. In the ore, vanadium was predominantly found in mica, with 67.4 wt.% occurring in roscoelite and 25.7 wt.% in sericite. Additionally, 6.8 wt.% of the vanadium was adsorbed on the surface of limonite. Furthermore, since 82.9 wt.% of vanadium exists in the form of trivalent vanadium, which is challenging to extract, the direct leaching method proves to be ineffective for efficient vanadium extraction. Roasting to facilitate the breakdown of the crystal lattice and the oxidation of vanadium presents a viable alternative.

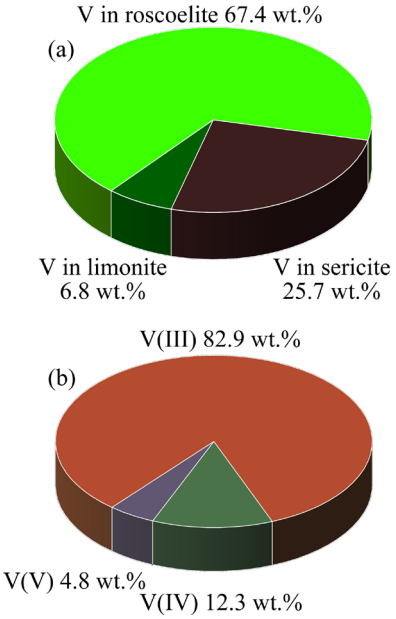

Fig. 3 Distribution (a) and valence state (b) of V in V-bearing shale

3.1.3 Embedded features of main minerals

The degree of dissociation and the intergrowth relationships of different minerals directly influence the difficulty and efficiency of subsequent processing steps. The particle size, dissociation degree, intergrowth relationships, micro-morphology, and embedded features of the primary minerals were analyzed using MLA and SEM, with the results presented in Figs. 4, 5, and 6. Figure 4(a) shows that the embedded particle size of primary minerals in the ore is relatively fine, predominantly distributed at −38 μm. Specifically, within the particle

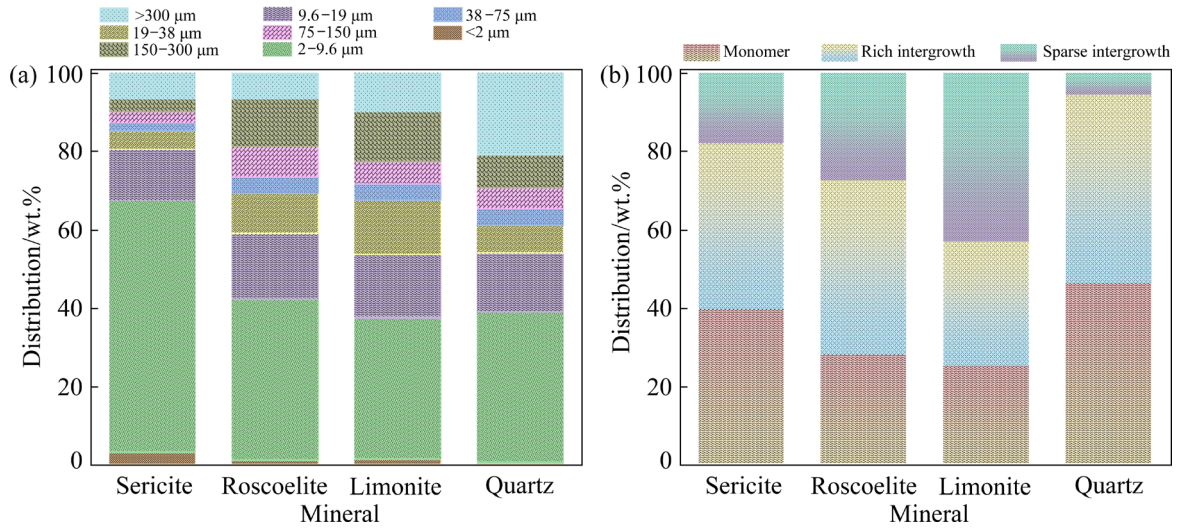

Fig. 4 (a) Embedded particle size distribution of primary minerals; (b) Degree of liberation for sericite, vanadium-bearing sericite, limonite, and quartz (Sparse intergrowth: 0%−50%; Rich intergrowth: 50%−100%; Monomer: 100%)

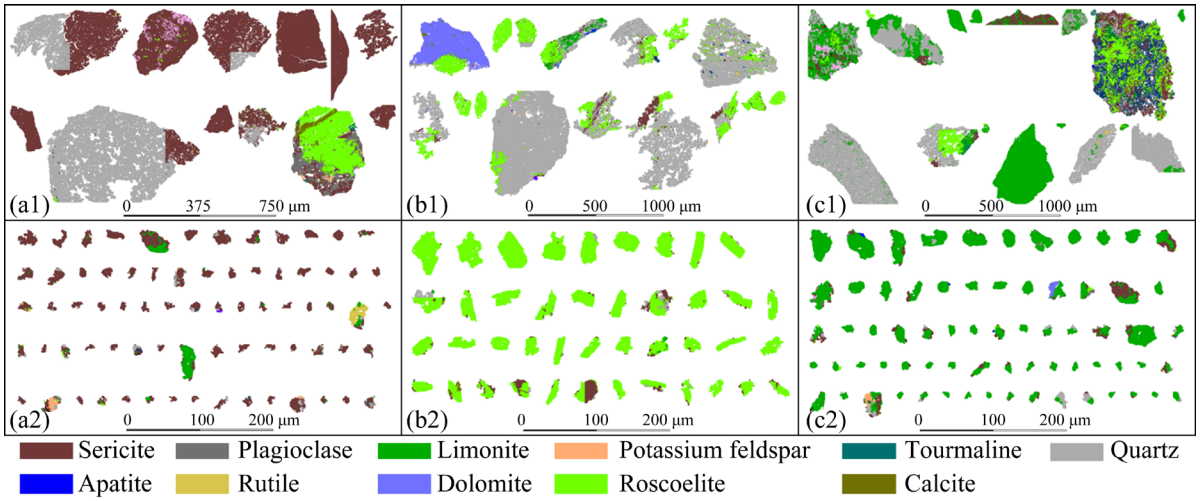

Fig. 5 Schematic diagrams of dissociation and intergrowth relationships among main minerals; (a_1, a_2) Sericite; (b_1, b_2) Roscoelite; (c_1, c_2) Limonite; (a_1, b_1, c_1) >38 μm; (a_2, b_2, c_2) <38 μm

size range of 2−9.6 μm, the highest concentrations were observed for sericite, roscoelite, limonite, and quartz, with distribution rates of 64.41, 41.13, 36.10, and 38.47 wt.%, respectively.

Figures 4(b), 5 and 6 reveal that the sericite monomer content is 39.48%, with rich intergrowths (greater than 50%) comprising 42.55% and sparse intergrowths (less than 50%) at 17.87%. Sericite appears as fine scaly aggregates either located between carbonaceous or quartz grains, or closely associated with quartz, limonite, roscoelite, and rutile. Sericite monomers frequently encapsulate small amounts of quartz, plagioclase, potassium feldspar, calcite, apatite, roscoelite, glauconite, tourmaline, rutile, and limonite. The encapsulated sericite was primarily surrounded by quartz among other minerals, and the rich intergrowths contained a substantial amount of quartz.

Roscoelite monomers, as well as rich and sparse intergrowths were present at 27.90%, 44.75%, and 26.97%, respectively. Roscoelite predominantly formed fine flaky aggregates and was closely associated with tourmaline, quartz, and carbonaceous materials. A small proportion of roscoelite crystals were well-formed, exhibiting hypidiomorphic textures, and coexisted closely with barite, apatite, rutile, quartz, and carbonaceous materials. Roscoelite monomers typically encapsulated small amounts of sericite, while the encapsulated roscoelite was predominantly

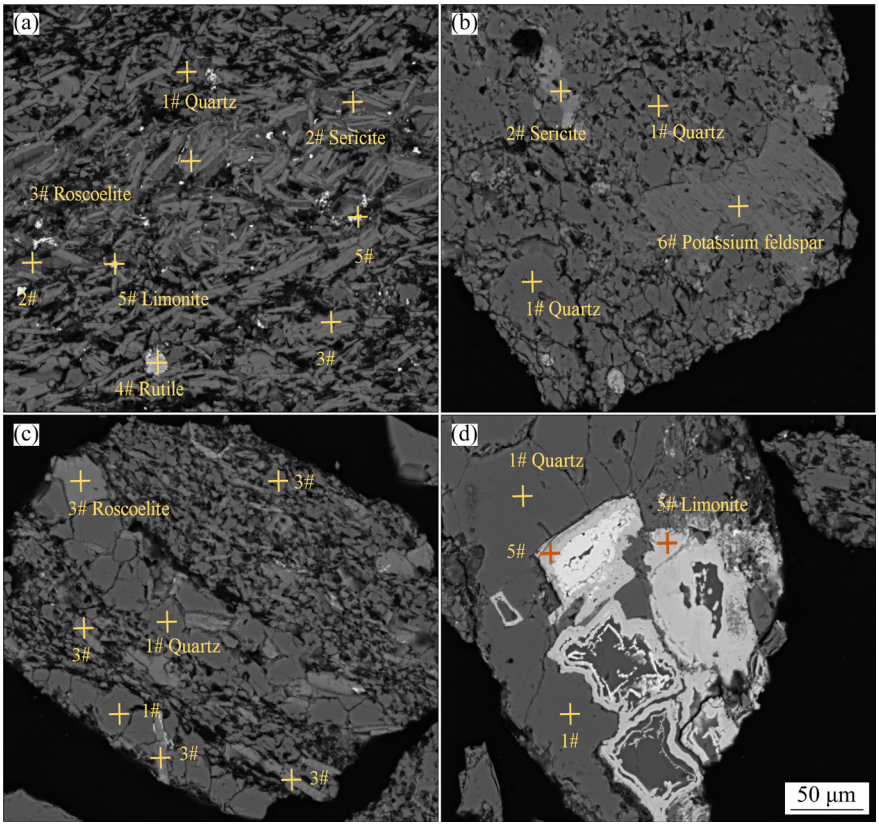

Fig. 6 Embedded characteristics of primary minerals: (a) Sericite and roscoelite; (b) Sericite; (c) Roscoelite; (d) Limonite

surrounded by quartz and sericite. The rich intergrowths contained a substantial proportion of sericite.

Limonite monomers, as well as rich and sparse intergrowths were present at 25.05%, 31.85%, and 41.96%, respectively. Limonite exhibited hypidiomorphic granular forms, pyritohedral shapes, and sparse disseminated patterns, or colloform appeared along rock fractures. Isolated limonite monomers enclosed quartz−sericite−roscoelite micro-inclusions. These inclusions formed quartz−sericite boundaries around limonite cores. Rich intergrowths within the limonite contained a substantial proportion of sericite.

Consequently, traditional beneficiation methods are insufficient for liberating V-bearing minerals and extracting vanadium. This work compares the effects of suspension oxidation roasting−direct leaching (SORDL) and suspension oxidation roasting−curing−leaching (SORCL) processes on vanadium extraction from V-bearing shales.

3.2 Pilot-scale SOR evaluation

3.2.1 Operational stability

A stable operation test was conducted under fixed conditions to assess the operational stability of the suspension roasting furnace. The stable operation conditions of the roasting process were set as follows: feeding rate of 30 kg/h, air gas flow of 28.0 m^3/h, O_2 gas flow of 4.0 m^3/h, and temperature of 900 °C in both the primary (suspension furnace) and secondary (fluidized reactor) reactors. The experiment was conducted under stable conditions for 48 h, with samples taken hourly for direct leaching tests. The leaching conditions were as follows: 40 wt.% acid usage, 8 h leaching time, and 90 °C leaching temperature. Figure 7 illustrates the leaching indicators, as well as the temperature and pressure of the key components during the continuous and stable operation of the suspension roasting system. The results shown in Fig. 7(a) indicate that product quality remained stable throughout the entire continuous operation. The average leaching efficiency of V_2O_5 and the average V_2O_5 grade in leaching slag were 67.15 and 0.37 wt.%, respectively. As shown in Fig. 7(b), throughout the continuous operation, the temperature and pressure of key components in the suspension roasting system, including the suspension furnace, fluidized

reactor, Roots blower, and cooler, remained stable.

After the experiment, the major components of the suspension roasting system that could experience blockage, wall adhesion, and ring formation were inspected, as shown in Fig. 8. It was observed that no wall adhesion or ring formation occurred inside the suspension furnace, and the inner walls of the fluidized reactor remained clean, indicating that no material adhesion occurred on the inner walls during the experiment.

3.2.2 Chemical composition analysis of ash and flue gas

During the suspension roasting process, ash is inevitably generated. To fully utilize this material, a chemical composition analysis was performed, and the results are presented in Table 3. It is evident that the composite ash contains 0.93 wt.% V_2O_5, with the main impurities being SiO_2 and Al_2O_3, which account for 62.77 and 6.66 wt.% respectively, and a carbon content of 12.80 wt.%. This indicates that the composite ash is a valuable vanadium-containing raw material and should be returned to the suspension roasting system for recycling in actual industrial production.

During the stable operation of the suspension roasting process, the emissions of atmospheric pollutants, such as sulfur dioxide (SO_2) and nitrogen oxides (N_xO_y) in the exhaust flue gas were monitored, and the results are presented in Table 4. It was found that the measured concentrations of PM, SO_2, N_xO_y, and carbon monoxide (CO) were 6.92, 57, 85, and 495 mg/m^3, respectively. Therefore, the flue gas from the vanadium-bearing shale suspension roasting contains gaseous pollutants such as PM, sulfur, nitrogen, and CO. The flue gas underwent baghouse dust removal in the roasting system, resulting in a solid particle concentration of only 6.92 mg/m^3, meeting the

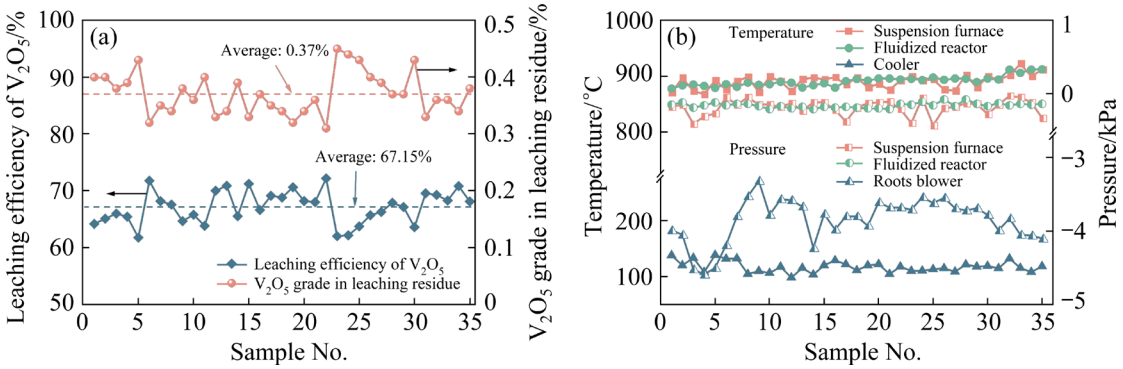

Fig. 7 Results of continuous operation stability test on suspension oxidation roasting process: (a) Leaching indicator; (b) Temperature and pressure of key components

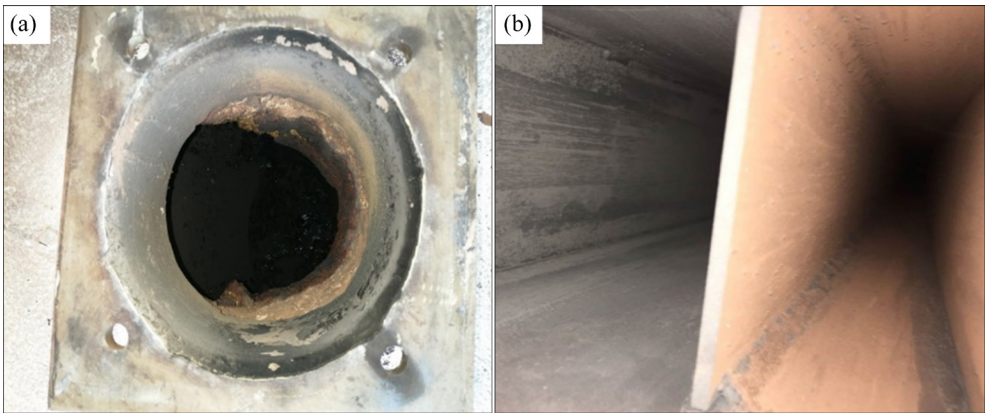

Fig. 8 Photos of inner walls of suspension furnace (a) and fluidized reactor (b)

Table 3 Chemical composition of comprehensive ash (wt.%)

Al_2O_3	SiO_2	V_2O_5	C	TFe	MgO	CaO	P	S	K	Na	LOI
6.66	62.77	0.93	12.80	2.30	1.03	3.24	0.26	0.35	1.70	0.47	14.95

Table 4 Flue gas test results

Component	Concentration/(mg·m^{-3})
PM*	6.92
SO_2	57
N_xO_y	85
CO	495

* PM: Particulate matter

requirement of the Gansu Province Industrial Furnace Air Pollution Comprehensive Treatment Implementation Plan (December 24, 2019), which states that particulate emissions should not exceed 10 mg/m^3. Sulfur in the flue gas can be efficiently removed using the gypsum method, meeting the requirement of the Gansu Province Industrial Furnace Air Pollution Comprehensive Treatment Implementation Plan (December 24, 2019), which states that SO_2 emissions should not exceed 35 mg/m^3. The nitrogen oxides concentration in the flue gas was below 100 mg/m^3, meeting the requirement of the Gansu Province Industrial Furnace Air Pollution Comprehensive Treatment Implementation Plan (December 24, 2019) that nitrogen oxide emissions should not exceed 100 mg/m^3, so denitrification was not required. The content of CO in the flue gas was 495 mg/m^3, equivalent to a volume concentration of 0.04%, which was well below the upper limit concentration of CO in flue gas during alumina and cement roasting production (2%), so no treatment was required.

3.3 Direct leaching of roasted products

Direct leaching tests were conducted on pilot-scale roasted products to determine the optimal leaching conditions, as shown in Fig. 9. Subsequent comparisons of the indices were made on this basis when acid curing−water leaching was applied.

The particle size of raw materials significantly impacts both the solid−liquid interface area and the viscosity of the slurry. As illustrated in Fig. 9(a), an increase in the grinding fineness led to a gradual increase in the V_2O_5 leaching efficiency. When the content of particles smaller than 0.074 mm increased from 60 to 90 wt.%, the V_2O_5 leaching efficiency rose from 66.50% to 72.08%. Due to the challenges of filtering and dewatering with excessive grinding fineness, an optimal grinding fineness of 90 wt.% for particles smaller than 0.074 mm was established.

The acid dosage determines the efficiency, selectivity, and extent of the leaching reaction. As shown in Fig. 9(b), the V_2O_5 leaching efficiency exhibited a gradual upward trend with the increase in leaching acid dosage. The leaching efficiency of V_2O_5 increased from 61.29% to 74.52% as the acid dosage increased from 35 to 50 wt.%. Moreover, a leaching efficiency of V_2O_5 exceeding 70% was achieved with an acid dosage exceeding 40%. Taking into account both economic considerations and leaching indices, the optimal acid usage was set at 40%.

Optimization of leaching time requires balancing the reaction rate and degree of completion to maximize metal recovery and economic benefits. Figure 9(c) shows that the V_2O_5 leaching efficiency initially increased with extended leaching time but subsequently decreased. Specifically, when the leaching duration was extended from 3 to 8 h, the V_2O_5 leaching efficiency increased from 62.93% to 72.08%. However, further extending the leaching time to 10 h resulted in a decrease in the V_2O_5 leaching efficiency to 68.24%. This reduction may be attributed to prolonged leaching at high temperatures, causing volatilization of water in the solution, ultimately leading to supersaturation and precipitation of V^{5+}. Consequently, the optimal leaching time was set at 8 h.

In the blank roasting−acid leaching process of vanadium ore, the addition of the leaching aid calcium fluoride aims to improve the efficiency and selectivity of acid leaching, but its environmental impact and economic costs must also be considered. As shown in Fig. 9(d), the V_2O_5 leaching efficiency progressively increased with the dosage of the leaching aid. Specifically, when the leaching aid dosage increased from 0% to 3%, the V_2O_5 leaching efficiency increased from 72.08% to 78.37%. The experimental results indicate that adding the leaching aid facilitates the leaching of V_2O_5.

Chemical composition analysis of the leaching residue under optimal conditions was performed, and the results are presented in Table 5. Following the blank roasting−direct acid leaching process, the content of V_2O_5 in the leaching residue decreased from 0.93 wt.% in the raw ore to 0.28 wt.%, the carbon content reduced from 12.40 to 0.074 wt.%,

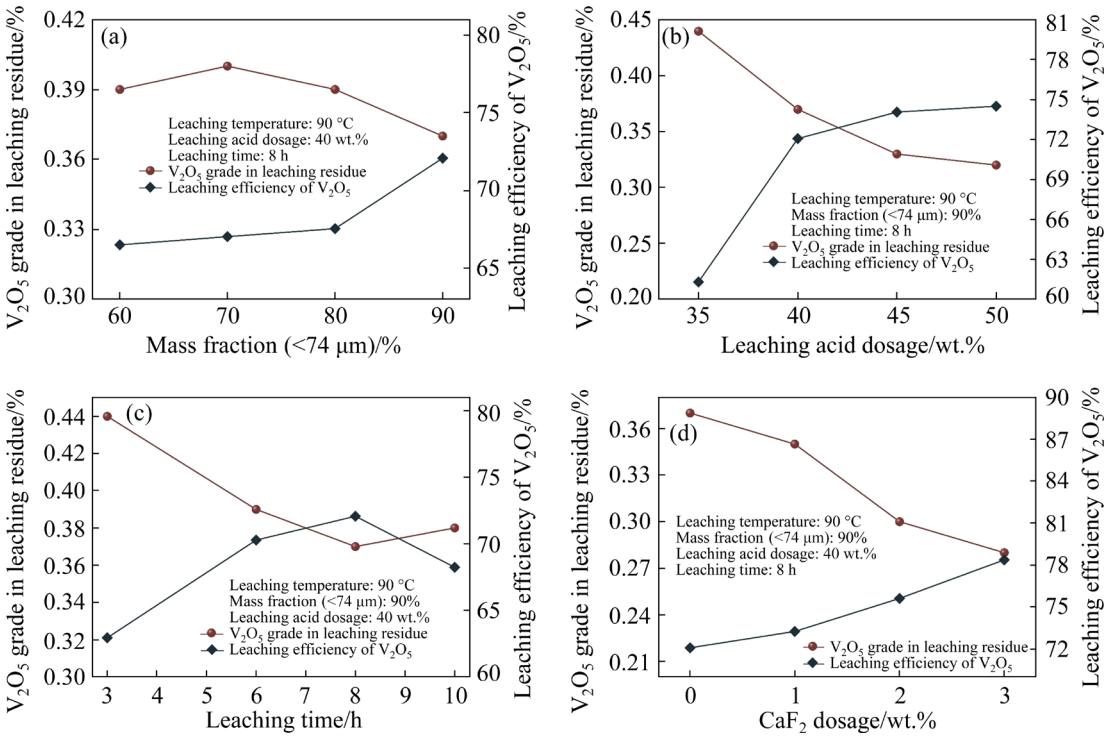

Fig. 9 Effect of process parameters on direct leaching of roasted products: (a) Grinding fineness; (b) Leaching acid dosage; (c) Leaching time; (d) CaF_2 dosage

Table 5 Chemical composition of leaching residue under optimal conditions for roasting−direct leaching process (wt.%)

Al_2O_3	SiO_2	V_2O_5	TiO_2	C	TFe	MgO	CaO	P	S	K	Na
3.50	76.85	0.28	0.95	0.074	1.49	0.45	2.35	0.044	1.40	0.92	0.28

the Al_2O_3 content decreased from 7.17 wt.% to 3.50 wt.%, and the content of the main impurity, SiO_2, increased from 58.79 to 76.85 wt.%.

3.4 Acid curing−water leaching of roasted products

While the direct leaching tests provided valuable insights into the leaching behavior of the roasted products, certain limitations were observed. These limitations included suboptimal leaching efficiency beyond 3 h. To address these challenges and enhance the overall extraction performance, the acid curing-water leaching method was investigated. The sulfuric acid curing-leaching process involves permeating concentrated sulfuric acid into the ore at a specific temperature, where it contacts minerals and undergoes oxidative reactions, converting trivalent vanadium (V(III)) into soluble tetravalent (V(IV)) and pentavalent (V(V)) forms. This is followed by a water leaching method to separate vanadium from the residue [42]. Compared to conventional methods, the curing−leaching process offers advantages, such as lower energy consumption, shorter operational cycles, and higher leaching efficiency [49]. Acid curing−water leaching tests were conducted on pilot-scale roasted products to determine optimal conditions, as shown in Fig. 10.

Reaction temperature is a critical parameter in the diffusion process [50]. Appropriate increase in temperature enhances the activity of atoms and molecules, accelerating the diffusion rate of sulfuric acid within the particles and improving the permeability of sulfuric acid in vanadium-bearing stone coal, facilitating the decomposition reactions of sericite/roscoelite [51]. However, excessively high temperatures not only increase energy consumption but also lead to secondary reactions of the transformed vanadium [41]. Therefore, selecting an appropriate curing temperature is necessary. As illustrated in Fig. 10(a), the V_2O_5 leaching efficiency initially increased, and then decreased. Upon the rise in curing temperature from 100 to

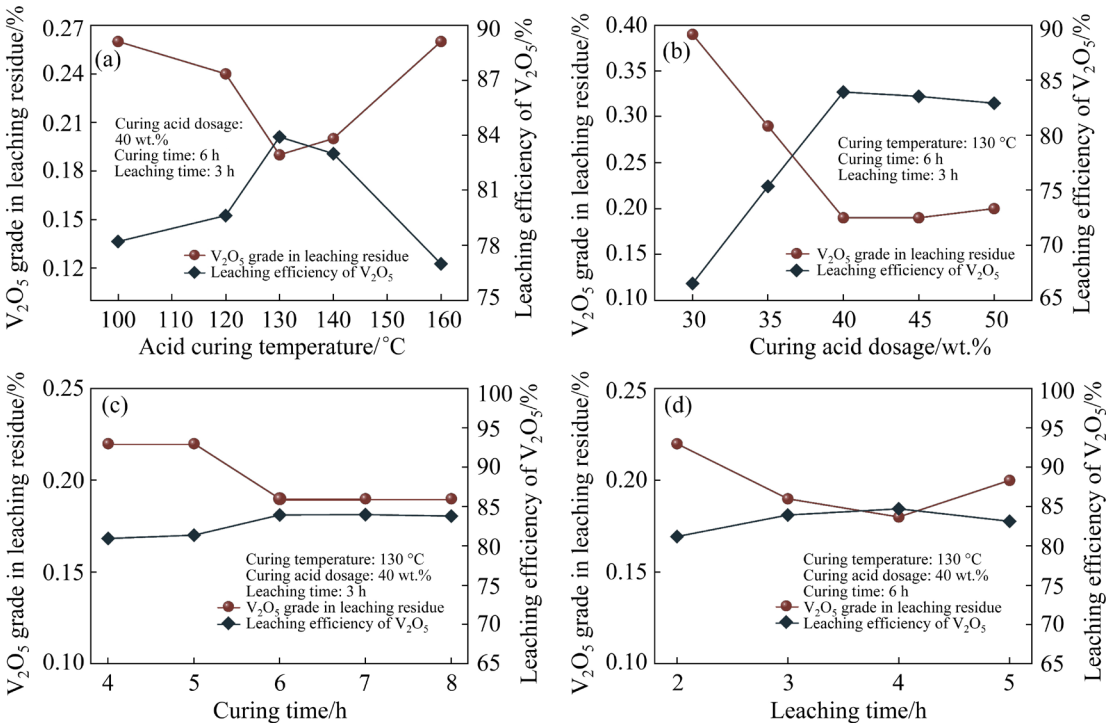

Fig. 10 Effect of process parameters on acid curing−water leaching process of roasted products: (a) Acid curing temperature; (b) Curing acid dosage; (c) Curing time; (d) Leaching time

130 °C, the leaching efficiency of V_2O_5 demonstrated an increase from 78.21% to 83.92%. Further increasing the temperature to 160 °C led to a decrease in the V_2O_5 leaching efficiency to 76.99%. This is due to intensified evaporation of water in the acid leaching system, increasing the viscosity of the slurry and consequently reducing the diffusion rate of sulfuric acid in the particles. Therefore, the optimal acid curing temperature is determined to be 130 °C.

Figure 10(b) indicates that as the curing acid dosage increased, the V_2O_5 leaching efficiency initially rose and then remained relatively stable. When the acid dosage increased from 30 to 40 wt.%, the V_2O_5 leaching efficiency rose from 66.52% to 83.92%. Further increasing the acid dosage did not significantly affect the V_2O_5 leaching efficiency, thus the optimal acid dosage was determined to be 40 wt.%.

Reaction time also plays a crucial role in the leaching process [52]. The goal is often to produce as much product as possible in the shortest time to maximize economic benefits for the industry. According to Fig. 10(c), the V_2O_5 leaching efficiency initially increased and then remained stable as the curing time was extended. When the curing time increased from 4 to 6 h, the V_2O_5 leaching efficiency rose from 80.93% to 83.92%. Further extension of the curing time did not significantly change the V_2O_5 leaching efficiency; thus, the optimal curing time was determined to be 6 h to conserve energy during production.

Figure 10(d) shows that as the water leaching time was extended, the V_2O_5 leaching efficiency initially increased and then remained relatively stable. When the leaching time increased from 2 to 4 h, the V_2O_5 leaching efficiency rose from 81.18% to 84.72%. Further extension of the leaching time caused the V_2O_5 leaching efficiency to fluctuate between 83.13% and 84.72%. When the leaching time exceeded 3 h, the V_2O_5 leaching efficiency consistently exceeded 83%. Considering energy consumption and leaching indicators, the optimal water leaching time was set at 3 h.

3.5 Comparative analysis of RCLR and RDLR

To compare the vanadium extraction efficiency of different processes, the chemical composition and mineral content of the raw ore, roasted products, direct leach residue (RDLR), and curing-leach residue (RCLR) were analyzed. The results are presented in Table 6 and Fig. 11. Table 6 shows that

Table 6 Chemical composition of raw ore and leaching residue from various processes (wt.%)

Sample	Al_2O_3	SiO_2	V_2O_5	TiO_2	C	TFe	MgO	CaO	P	S	K	Na
Raw ore	7.17	58.79	0.93	0.74	12.40	2.82	1.19	3.31	0.28	0.44	1.64	0.56
Roasted product	8.61	70.86	1.02	0.92	0.108	3.59	1.55	3.82	0.35	0.51	1.95	0.68
Direct acid leaching residue	3.50	76.85	0.28	0.95	0.074	1.49	0.45	2.35	0.044	1.40	0.92	0.28
Acid curing−leaching residue	3.52	78.35	0.19	0.63	0.089	1.20	0.51	1.28	0.073	1.01	1.08	0.42

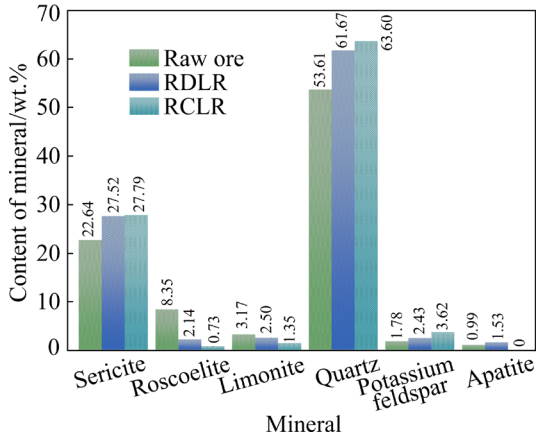

Fig. 11 Mineral contents of raw ore and leaching residue from various processes as determined by MLA

the sulfur content in the minerals decreased after roasting, while the carbon content decreased significantly. Due to the loss of carbon, the remaining chemical components increased to varying degrees. After leaching, the SiO_2 and S contents in the products increased significantly, and the TiO_2 content in the direct leach residue also rose. However, the remaining constituents decreased to varying extents. Compared to the direct leach residue, the curing−leach residue had higher SiO_2 and lower V_2O_5 and CaO contents, indicating that more vanadium- and calcium-bearing minerals were leached during the curing−leaching process. Figure 11 shows that the contents of roscoelite and limonite decreased significantly through the SORDL and SORCL processes, while the contents of other major minerals, such as sericite, quartz, and feldspar increased. This suggests that the majority of the leached vanadium originates from roscoelite and limonite. A comparative analysis of the apatite content indicates that the RCL process also facilitates apatite leaching. In conclusion, the SORCL process achieves better leaching indicators and is a more efficient method for vanadium extraction. Subsequent analysis of the products from the SORCL process will be conducted to elucidate the mechanisms of roasting and leaching.

3.6 Phase selective transition analysis

XRD analysis was conducted on raw ore, roasted products, and leach residue from the SORCL process. As illustrated in Fig. 12(a), the primary components of the raw ore were quartz and sericite. The diffraction peaks corresponding to limonite and calcite were weak, indicating their low content. After roasting, limonite dehydrated to form hematite, and calcite decomposed. The crystal structure of sericite was disrupted by the removal of —OH groups from the Al—O octahedra, transforming it into illite. Consequently, the diffraction peaks for these three substances in the roasted product disappeared. Following leaching, the diffraction peak for hematite weakened, with

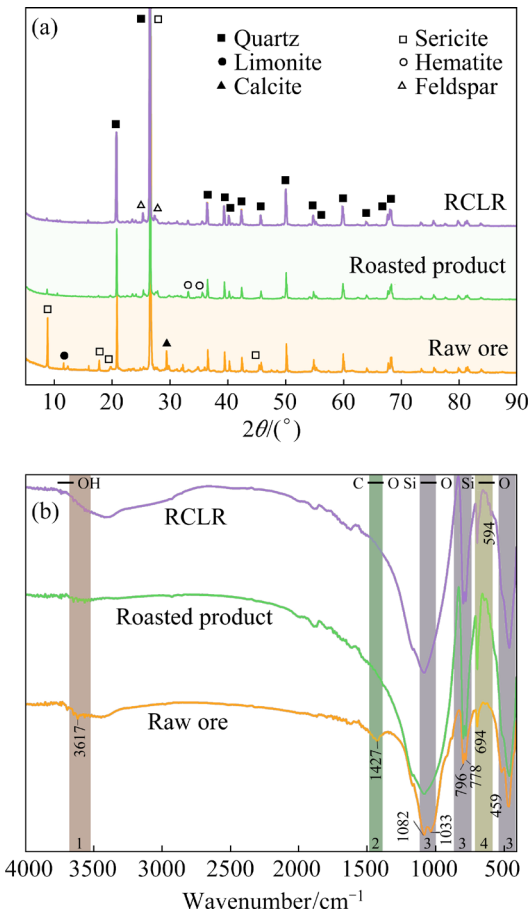

Fig. 12 XRD (a) and FT-IR (b) patterns of products at various stages of roasting−curing leaching

almost no change in the other peaks. Therefore, roasting was beneficial for disrupting the crystal structure of mica, thereby enhancing the leaching efficiency of vanadium.

FT-IR analysis was performed on the raw ore, roasted ore, and RCLR to verify the transformation or breaking of chemical bonds in minerals like mica. The results are presented in Fig. 12(b). According to Refs. [25,36], absorption band 1 (3614 cm^{-1}) in the infrared spectrum corresponds to the stretching vibration of O—H. Absorption band 2 (1427 cm^{-1}) corresponds to the bending vibration of C—O, characteristic of calcite and dolomite. Absorption band 3 (1082, 1033, 796, 778, and 459 cm^{-1}) corresponds to the bending vibrations of Si—O, which are characteristic of silicate minerals like mica. Absorption band 4 (694 cm^{-1}) represents the symmetric stretching vibration of Si—O, characteristic of quartz. After roasting, absorption bands 1 and 2 disappeared due to dehydroxylation and carbonate decomposition reactions occurring during roasting process. The disappearance of the absorption band at 1033 cm^{-1} indicates that roasting disrupted the Si—O tetrahedral and Al—O octahedral structures, altering the coordination numbers of Al and Si. These changes promoted the disruption of the layered mica structure. Following leaching, the intensity of the absorption band at 594 cm^{-1} exhibited a slight increase, indicating an increase in SiO_2 content.

3.7 Microstructure analysis

Figure 13 illustrates the microstructure of the primary minerals in the roasted products. It was evident that the major minerals in the roasted products exhibited significant changes in microstructure, accompanied by compositional transformations. The primary changes included the transformation of vanadium-bearing mica into illite−montmorillonite and limonite to hematite. The transformations between vanadium-bearing sericite and illite−montmorillonite occurred in the following three stages: (1) Vanadium-bearing mica exhibited xenomorphic-hypidiomorphic flaky structures, with coarse grain sizes ranging from 0.05 to 0.08 mm, closely intergrown with limonite and quartz. The crystal shapes showed deformations, appearing flexed and bent, with some flaky crystals being incomplete and having indistinct, blurred boundaries. However, the composition remained that of vanadium-bearing sericite. It is suggested that there may be a trend toward transformation to illite−montmorillonite during roasting (Figs. 13(a) and (b)). (2) Vanadium-bearing mica retained its xenomorphic-hypidiomorphic flaky crystal forms, with finer grains smaller than 0.02 mm in length. However, the composition had transformed into illite−montmorillonite or exhibited a transitional

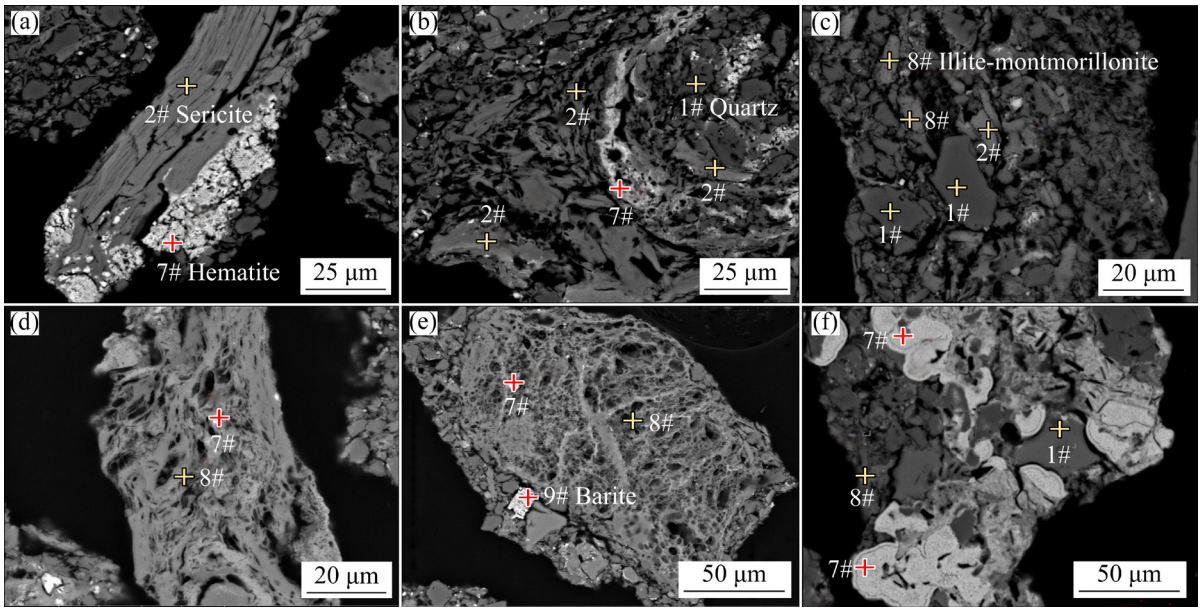

Fig. 13 Embedded features of vanadium-bearing mica (sericite and roscoelite) (a−c), illite−montmorillonite (d, e), and limonite (f)

state between illite−montmorillonite and vanadium-bearing sericite (Figs. 13(c) and (d)). In raw ore, illite−montmorillonite appeared as irregular thin flakes, almost lacking distinct crystal forms. Therefore, it is speculated that the minerals retaining the hypidiomorphic flaky crystal morphology but composed of illite−montmorillonite are derived from the transformation of vanadium-bearing sericite during roasting. (3) The crystal form of vanadium-bearing sericite was incomplete, appearing irregular. Sericite is primarily intergrown with illite−montmorillonite in a clustered habit, and secondarily, closely associated with quartz and barite (Fig. 13(e)). This represents the complete transformation of vanadium-bearing sericite into illite−montmorillonite. Another vanadium-bearing mineral, limonite, has primarily transformed into hematite compositionally. Microstructurally, limonite was predominantly distributed in a colloidal form, closely intergrown with quartz, vanadium-bearing sericite, and illite−montmorillonite (Fig. 13(f)).

Figure 14 presents the N_2 adsorption−desorption isotherms, pore size distribution, and pore characteristics analysis results for the raw ore, roasted products, and RCLR. It is evident that the isotherms of the three samples belong to the H3 type, and the pores are predominantly mesopores (medium-sized pores) with sizes ranging from 2 to 50 nm. H3-type isotherms typically appear in layered clay particles and are characterized by slit-shaped pores. Following the roasting process, the maximum adsorption capacity of the product exhibited a notable decline, decreasing from 21.0207 to 3.3381 cm^2/g. However, after subjecting the roasted product to leaching, the maximum adsorption capacity demonstrated an increase, reaching 8.9468 cm^2/g. The analysis results for total pore volume and specific surface area are consistent to those for maximum adsorption capacity. After roasting, both the total pore volume and specific surface area of the product showed a significant decrease. Following leaching, both metrics showed

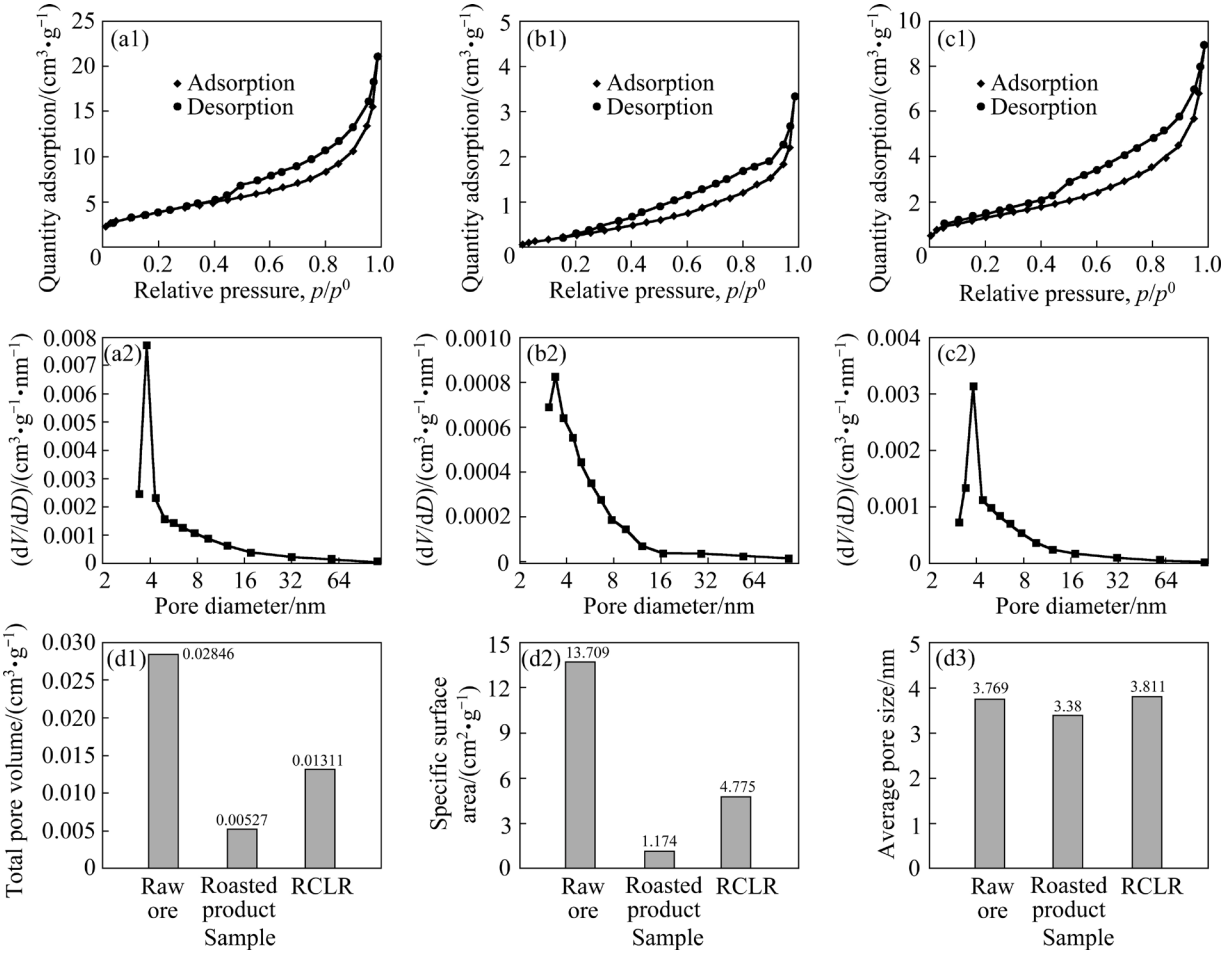

Fig. 14 Adsorption−desorption isotherms of N_2 (a1, b1, c1) and pore size distribution (a2, b2, c2) of raw ore (a1, a2), roasted products (b1, b2) and RCLR (c1, c2), total pore volume (d1), specific surface area (d2), and average pore size (d3)

a significant increase. The average pore size did not show any significant change. This was due to the reaction of CaO, produced by the decomposition of calcite and dolomite during roasting, with mica, forming a silicate mineral-based coating and sealing some cracks and pores [53]. This led to a decrease in the number of pores, while the pore size did not change significantly. However, during the leaching process, the coating is partially destroyed, exposing some cracks and pores.

4 Conclusions

(1) The ore contained 0.93 wt.% V, primarily as V(III) in sericite, roscoelite, and limonite.The main vanadium-bearing minerals exhibited fine embedded particle sizes, low degrees of individual mineral liberation, and complex intergrowth relationships. These factors present significant challenges to vanadium extraction. Therefore, promoting lattice destruction and vanadium oxidation through suspension oxidation roasting to enhance subsequent leaching is a feasible approach.

(2) Under continuous operation, the suspension roasting system, including the suspension furnace and fluidized reactor, exhibited stable working conditions with stable and reliable production operation. A comparative analysis of the SORDL and SORCL processes revealed that the latter exhibited superior leaching efficiency, and the leaching efficiency of vanadium can reach 83.92%.

(3) Mechanistic analysis indicated that vanadium-bearing mica underwent dehydroxylation and transformed into illite−montmorillonite during roasting. However, the transformation was incomplete, with some remaining in a transitional state. These changes disrupted the crystal structure of mica, facilitating vanadium extraction. At elevated temperatures, the roasted products exhibited sintering, sealing some cracks and pores. During the subsequent leaching process, some of these cracks and pores were reopened.

CRediT authorship contribution statement

Zhe BAI: Validation, Formal analysis, Data curation; **Jia-hao HE:** Writing – Original draft, Validation, Formal analysis; **Ming-xing WANG:** Supervision, Methodology; **Yue-xin HAN:** Writing − Review & editing, Conceptualization; **Yong-sheng SUN:** Conceptualization, Methodology; **Shuai YUAN:** Resources, Project administration, Funding acquisition; **Jian-ping JIN:** Resources, Project administration, Funding acquisition.

Declaration of competing interest

The authors declare that they have no known competing financial interests or personal relationships that could have appeared to influence the work reported in this paper.

Acknowledgments

This research is funded by the National Key Research and Development Program of China (No. 2020YFC1909704), and the Fundamental Research Funds for the Central Universities, China (Nos. N2301026, N2301017).

References

[1] LIU Shi-yuan, WANG Li-jun, CHEN Jun, YE Liu, DU Jun-yan. Research progress of vanadium extraction processes from vanadium slag: A review [J]. Separation and Purification Technology, 2024, 342: 127035.

[2] LI Chang-qing, JIANG Tao, WEN Jing, YU Tang-xia, LI Fei-fei. Review of leaching, separation and recovery of vanadium from roasted products of vanadium slag [J]. Hydrometallurgy, 2024, 226: 106313.

[3] YAN Zheng-pei, ZHENG Shi-li, ZHANG Ying, ZHANG Yang, ZHOU Zhen-gen, QIAO Shao. Sodium carbonate roasting and mild acid leaching of vanadium titanomagnetite concentrates: Vanadium extraction and residue sodium decrease [J]. Process Safety and Environmental Protection, 2024, 185: 1132−1144.

[4] LIU Hong, ZHANG Yi-min, LIU Tao, HUANG Jing, CHEN Li-ming, HU You-wen. Preparation of vanadium electrolyte from vanadium shale leaching solution with high concentration chloride using D2EHPA [J]. Transactions of Nonferrous Metals Society of China, 2023, 33(5): 1594−1608.

[5] ISHAQ M A, YASIR M, MEGAT YUSOFF P S M, TARIQ A, SARIKAYA M, KHAN M S. MXenes-enhanced vanadium redox flow batteries: A promising energy solution [J]. Journal of Energy Storage, 2024, 96: 112711.

[6] AN Ya-rui, MA Bao-zhong, LI Xiang, CHEN Yong-qiang, WANG Cheng-yan, WANG Bao-hua, GAO Ming-lei, FENG Guo-sheng. A review on the roasting-assisted leaching and recovery of V from vanadium slag [J]. Process Safety and Environmental Protection, 2023, 173: 263−276.

[7] ZHANG Shu-shi, WANG Zhen-yang, HU Peng, RAO Jia-ting, ZONG Yan-bing, PANG Jing. Influence of composition and temperature on distribution behavior of V,

Ti and Si in HIsmelt [J]. Transactions of Nonferrous Metals Society of China, 2023, 33(12): 3835−3846.

[8] HE Ye, ZHANG Yi-ming, ZHENG Qiu-shi, HUANG Jing, LIU Hong, ZHANG Liu-hong. Simultaneous stripping and regeneration of chelate structure of vanadium through vanadium reduction and conversion in vanadium-bearing shale extraction [J]. Journal of Environmental Chemical Engineering, 2023, 11(5): 110923.

[9] JIA Yong-zheng, QING Yu, FENG Bao-yan, ZHONG Yi-wei, DAI Lei, WANG Ming-yong. Green redox separation and efficient extraction of vanadium and chromium from leaching solution of chrome-vanadium slag [J]. Separation and Purification Technology, 2024, 343: 127098.

[10] ZHU Xin-ran, YANG Shuai-hou, ZHOU Zhen-ya, JIN Jian-ping, HAN Yue-xin. A sustainable method for high-efficient exploitation of low-grade vanadium-bearing shale ore by oxidation roasting pretreatment [J]. Journal of Cleaner Production, 2024, 447: 141627.

[11] CHENG Jie, LI Hong-yi HAI Dong, CHEN Xin-mian, DIAO Jiang, XIE Bing. Acidic leaching kinetics study on vanadium from magnesiation-roasted vanadium slag [J]. Transactions of Nonferrous Metals Society of China, 2024, 34(2): 669−680.

[12] BAI Zhe, HAN Yue-xin, JIN Jian-ping, SUN Yong-sheng, ZHOU Zhen-ya. Extraction of vanadium from black shale by novel two-step fluidized roasting process [J]. Powder Technology, 2022, 408: 117745.

[13] YUAN Yi-zhong, ZHANG Yi-min. Improvement of the grindability of vanadium-bearing shale and the direct vanadium leaching efficiency of grinded product via microwave pretreatment with particle size classification [J]. Colloids and Surfaces A: Physicochemical and Engineering Aspects, 2022, 647: 128979.

[14] ZUO Peng-fei, CHEN Qiang, XIAO Zi-han, DONG Yi-ming, SUN Jiang-tao, SUN Xue-fei, LIU Lei. Geology and mineral assemblages of the early Cambrian black shales in the South Qinling: Implications for vanadium and barium mineralization [J]. Ore Geology Reviews, 2023, 161: 105624.

[15] VIND J, TAMM K. Review of the extraction of key metallic values from black shales in relation to their geological and mineralogical properties [J]. Minerals Engineering, 2021, 174: 107271.

[16] RAINOLDI A L, BEAUFORT D, FRANCHINI M B, GIUSIANO A, PETIT S, PATRIER P, PONS M J. Vanadium mineralization at Los Chihuidos sediment-hosted Cu−V deposit, Neuquén Basin, Argentina: An approach to vanadium ore forming processes [J]. Geoscience Frontiers, 2024, 15(1): 101724.

[17] ZHAO Xu-xia, ZHANG Yi-min, XUE Nan-nan, HU Peng-cheng, ZHENG Qiushi, HU Yibo. Effect of mechano-chemical activation with NaF on improved acid leaching of vanadium-bearing shale [J]. Hydrometallurgy, 2023, 221: 106126.

[18] TAO Yuan-yuan, YE Guo-hua, ZHANG Hao, WANG Xiao, ZUO Qi. The oxidation behavior of MnO_2 on the surface of a shale vanadium ore [J]. Colloids and Surfaces A: Physicochemical and Engineering Aspects, 2023, 677: 132327.

[19] ZHENG Qiu-shi, ZHANG Yi-min, LIU Tao, HUANG Jing, XUE Nan-nan. Vanadium extraction from black shale: Enhanced leaching due to fluoride addition [J]. Hydrometallurgy, 2019, 187: 141−148.

[20] ZHENG Qiu-shi ZHANG Yi-min, XUE Nan-nan. Migration and coordination of vanadium separating from black shale involved by fluoride [J]. Separation and Purification Technology, 2021, 266: 118552.

[21] ZHENG Qiu-shi, ZHANG Yi-min, XUE Nan-nan. Enhancing effect of vanadium releasing efficiently from lattice in black shale by thermal activation [J]. Colloids and Surfaces A: Physicochemical and Engineering Aspects, 2022, 651: 129773.

[22] CHEN Bo, BAO Shen-xu, ZHANG Yi-min. Synergetic strengthening mechanism of ultrasound combined with calcium fluoride towards vanadium extraction from low-grade vanadium-bearing shale [J]. International Journal of Mining Science and Technology, 2021, 31(6): 1095−1106.

[23] CHEN Bo, BAO Shen-xu, ZHANG Yi-min, LI Sheng. A high-efficiency and sustainable leaching process of vanadium from shale in sulfuric acid systems enhanced by ultrasound [J]. Separation and Purification Technology, 2020, 240: 116624.

[24] CHEN Bo, BAO Shen-xu, ZHANG Yi-min. Effects of key impurities (Al, Fe, P, Si and Na) on the precipitation process of vanadium in the novel ultrasound-assisted precipitation system [J]. Hydrometallurgy, 2024: 224: 106233.

[25] MENG Rui, LIU Tao, ZHANG Yi-min, HUANG Jing, YUAN Yi-zhong, HU Peng-cheng. Synchronous activation of Si and Al in vanadium-bearing shale leaching residue via sodium carbonate additive [J]. Construction and Building Materials, 2018, 170: 20−25.

[26] LI Wang, MA Chen, GONG Wen-hui, ZHU Xiao-bo. Clean production technology for effective recovery of vanadium from shale: Interaction between activators and vanadium-loaded minerals [J]. Journal of Cleaner Production, 2021, 315: 128170.

[27] HU Peng-cheng, ZHANG Yi-min. Efficient vanadium extraction from shale with high silicon content using a short flow process by roasting-water leaching: Laboratory and industrial scale research [J]. Silicon, 2022, 14(7): 3775−3784.

[28] WANG Bo, LIU Tao, ZHANG Yi-min, HUANG Jing. Effect of CaF_2/CaO composite additive on roasting of vanadium-bearing stone coal and acid leaching kinetics [J]. Minerals, 2017, 7(3): 43.

[29] XUE Nan-nan, ZHANG Yi-min, LIU Tao, ZHENG Qiu-shi. Efficient separation of black shale-hosted vanadium induced by formation of kalunite−jarosite solid solution in two-stage pressurized acid leaching coupled with lixivium recycling [J]. Separation and Purification Technology, 2021, 269: 118762.

[30] LIU Shu-gen, DING Er-mao, NING Ping, XIE Gang, YANG Ni. Vanadium extraction from roasted vanadium-bearing steel slag via pressure acid leaching [J]. Journal of Environmental Chemical Engineering, 2021, 9(3): 105195.

[31] CAI Zhen-lei, WANG Yue, ZHANG Yi-min, ZHENG Qiu-shi. Improvement on bioleaching interfacial behavior

between Bacillus mucilaginosus and vanadium-bearing shale by surfactant additive [J]. Journal of Environmental Chemical Engineering, 2022, 10(6): 108911.

[32] CAI Zhen-lei, WANG Yue, ZHANG Yi-min, TIAN Hong-qing. Effects of surfactant on Bacillus mucilaginosus adsorption characteristics during vanadium bioleaching process [J]. Journal of Environmental Chemical Engineering, 2022, 10(6): 108961.

[33] CAI Jin-peng, SHEN Pei-lun, LIU Dian-wen, ZHANG Xiao-lin, FANG Jian-jun, SU Chao, YU Xing-cai, LI Jiang-li, WANG Han. Growth of covellite crystal onto azurite surface during sulfurization and its response to flotation behavior [J]. International Journal of Mining Science and Technology, 2021, 31(6): 1003−1012.

[34] ZENG Xi, WANG Fang, ZHANG Hui-feng, CUI Li-jie, YU Jian, XU Guang-wen. Extraction of vanadium from stone coal by roasting in a fluidized bed reactor [J]. Fuel, 2015, 142: 180−188.

[35] CAO Yue, SUN Yong-sheng, GAO Peng, HAN Yue-xin, LI Yan-jun. Mechanism for suspension magnetization roasting of iron ore using straw-type biomass reductant [J]. International Journal of Mining Science and Technology, 2021, 31(6): 1075−1083.

[36] ZHOU Zhen-ya, ZHU Yi-min, JIN Jian-ping HAN Yue-xin, BAI Zhe, TANG Zhi-dong. Enhanced vanadium extraction from Muscovite-type Vanadium-bearing shale by suspension oxidation roasting pretreatment-acid leaching [J]. Separation and Purification Technology, 2023, 309: 123066.

[37] YUAN Shuai, QIN Yong-hong, JIN Yong-peng, LI Yan-jun. Improving vanadium extraction from refractory stone coal by suspension roasting [J]. Transactions of Nonferrous Metals Society of China, 2023, 33(3): 902−916.

[38] YUAN Shuai, QIN Yong-hong, JIN Yong-peng, LI Yan-jun. Suspension roasting process of vanadium-bearing stone coal: Characterization, kinetics and thermodynamics [J]. Transactions of Nonferrous Metals Society of China, 2022, 32(11): 3767−3779.

[39] JIN Jian-ping, YU Xiao-long, BAI Zhe, ZHOU Zhen-ya, HAN Yue-xin, LI Yan-jun. The effect and mechanism analysis of calcium and magnesium between the blank roasting-leaching process of vanadium shale [J]. Fuel, 2025, 396: 135320.

[40] BAI Zhe, SUN Yong-sheng, XU Xu, JIN Jian-ping, HAN Yue-xin. A novel process of gradient oxidation roasting-acid leaching for vanadium extraction from stone coal [J]. Advanced Powder Technology, 2024, 35(1): 104296.

[41] LI Hui, HAN Yue-xin, JIN Jian-ping, ZHOU Zhen-ya. New insights into the penetration depth of sulfuric acid and leaching effect in the sulfuric acid curing-leaching process of vanadium-bearing stone coal [J]. ACS Omega, 2021, 6(27): 17599−17608.

[42] WANG Ming-yu, XIANG Xiao-yan, ZHANG Li-ping, XIAO Lian-sheng. Effect of vanadium occurrence state on the choice of extracting vanadium technology from stone coal [J]. Rare Metals, 2008, 27(2): 112−115.

[43] LIU Wan-li, WANG Xue-wen, WANG Ming-yu, HU Jian, ZHANG Li-ping. Mineral decomposition process of vanadium recovery from stone coal by low temperature sulphating roasting [J]. The Chinese Journal of Nonferrous Metals, 2009, 19(5): 943−948. (in Chinese)

[44] NING Ji-lai, GAO Peng, YUAN Shuai, HAN Yue-xin, SUN Yong-sheng, LI Wen-bo. Highly efficient and green separation of iron from complex low-grade polymetallic ore via hydrogen-based mineral phase transformation [J]. Powder Technology, 2024, 433: 119177.

[45] WANG Ming-xing, ZHANG Qiang, SUN Yong-sheng, HAN Yue-xin, GAO Peng. Green iron recovery through hydrogen-based mineral phase transformation using ultrafast air-cooling for heat recycling: A pilot-scale investigation [J]. Journal of Cleaner Production, 2024, 450: 141867.

[46] ZHU Si-di, XIA Ming-zhu, CHU Yu-ting, KHAN M A, LEI Wu, WANG Feng-yun, MUHMOOD T, WANG A-long. Adsorption and desorption of Pb(II) on L-lysine modified montmorillonite and the simulation of interlayer structure [J]. Applied Clay Science, 2019, 169: 40−47.

[47] ZHENG Qiu-shi, ZHANG Yi-min, LIU Tao, HUANG Jing, XUE Nan-nan, SHI Qi-hua. Optimal location of vanadium in muscovite and its geometrical and electronic properties by DFT calculation [J]. Minerals, 2017, 7(3): 32.

[48] ZHOU Zhen-ya, JIN Jian-ping, ZHU Yi-min, HAN Yue-xin, LI Yan-jun, LI Hui. Process mineralogical characterization and vanadium extraction from vanadium-bearing shale by oxidation roasting-acid leaching [J]. Advanced Powder Technology, 2022, 33(11): 103834.

[49] LI Hui, HAN Yue-xin, JIN Jian-ping, GAO Peng, ZHOU Zhen-ya. Process mineralogy approach to optimize curing-leaching in vanadium-bearing stone coal processing plants [J]. International Journal of Mining Science and Technology, 2023, 33(1): 123−131.

[50] HE Jia-hao, GUO Lei, GAO Peng, ZHU Xin-ran, YUAN Shuai, WANG Zi-hang, HAN Yue-xin. Recovery of strategic mineral resources such as iron and rare earth from solid waste stockpiled for years: Low-temperature fluidized reduction process and hydrogen substitution for carbon [J]. Separation and Purification Technology, 2025, 360: 131233.

[51] PENG Hao, GUO Jing, ZHENG Xiao-gang, LIU Zuo-hua, TAO Chang-yuan. Leaching kinetics of vanadium from calcification roasting converter vanadium slag in acidic medium [J]. Journal of Environmental Chemical Engineering, 2018, 6(4): 5119−5124.

[52] HE Jia-hao, GAO Peng, YUAN Shuai, CHENG Shao-kai, NING Ji-lai, ZHOU Zhen-ya, SUN Yong-sheng, LI Wen-bo. High efficiency separation of bastnaesite ($REFCO_3$) and monazite ($REPO_4$) in mixed rare earth concentrate by heating under N_2 and leaching with $HCl/AlCl_3$ [J]. Hydrometallurgy, 2024, 228: 106338.

[53] YUAN Yi-zhong, ZHANG Yi-min, HU Peng-cheng. Formation mechanism and control method of the silicate minerals-based coating (SMC) in blank roasting process of vanadium-bearing shale [J]. Colloids and Surfaces A: Physicochemical and Engineering Aspects, 2020, 592: 124535.

悬浮氧化焙烧−熟化−浸出法从含钒页岩中提钒的中试研究

白 哲[1,2,3]，何佳昊[1,2]，王明星[1,2]，韩跃新[1,2]，孙永升[1,2]，袁 帅[1,2]，靳建平[1,2]

1. 东北大学 矿物加工科学与技术全国重点实验室，沈阳 110819；
2. 东北大学 资源与土木工程学院，沈阳 110819；
3. 低碳钢铁前沿技术教育部工程研究中心，沈阳 110819

摘 要：针对传统含钒页岩提钒方法存在的环保问题，提出一种高效清洁的悬浮氧化焙烧−熟化−浸出工艺，并进行半工业试验。原矿中钒主要赋存于绢云母、褐铁矿和赤铁矿中，且主要以 V(III)和 V(IV)形式存在。在给料速率 30 kg/h、空气流量 28.0 m^3/h、O_2 流量 4.0 m^3/h、悬浮炉和流化床反应器中的温度均为 900 ℃的条件下，含钒云母发生脱水，转化为伊利石−蒙脱石，破坏了云母的晶体结构，有利于钒的提取。与直接酸浸相比，熟化浸出工艺对钒的提取效果更佳。在熟化温度 130 ℃、酸用量 40%(质量分数)、熟化时间 6 h、浸出时间 3 h 的条件下，V_2O_5 浸出率可达 83.92%。

关键词：含钒页岩；悬浮焙烧；熟化浸出；试点案例；矿物学

(Edited by Xiang-qun LI)